京都大学防災研究所年報 第45号 B 平成14年4月
Annuals of Disas. Prev. Res. Inst., Kyoto Univ., No. 45 B, 2002

A Computational Method for Residual Excess Pore Pressure Response in Sand Under Cyclic Loading

Aurelian C. TRANDAFIR, Kyoji SASSA and Hiroshi FUKUOKA

Synopsis

This study is concerned with the formulation of a numerical procedure to evaluate the residual excess pore water pressure generated in sandy soils during cyclic loading. Undrained cyclic loading and drained monotonic ring shear tests on sand were examined and it was revealed that the residual excess pore pressure response during undrained loading conditions could be related to sample height changes in drained monotonic shearing. Consequently, an incremental calculation method for the residual excess pore water pressure changes under undrained conditions is proposed and calibrated against experimental results. Finally, the procedure was validated through comparison with results of an undrained cyclic loading ring shear test performed under both cyclic total normal stress and cyclic shear stress. The proposed method allows for theoretical computation of progressive increase of the residual excess pore water pressure during undrained cyclic loading using basic sand properties, and thus, it also provides the opportunity to couple such pore water pressure increases with the dynamic response analyses.

Keywords: excess pore pressure; residual excess pore pressure; ring shear tests; sandy soil; incremental analysis

1. Introduction

Earthquake-induced landslides represent a major concern in countries at high seismic risk, since they may be responsible for significant amounts of damage and casualties. When an earthquake occurs, the effects of earthquake-induced ground shaking is often sufficient to cause failure of slopes that were marginally to moderately stable before the earthquake (Kramer, 1996). Earthquake-induced landslides in slope materials susceptible to shear strength reduction, such as saturated sandy soils, may turn into flow slides if the amount of earthquake-induced loss in shear strength is large enough to bring the available soil shear resistance below the in-situ gravitational shear stress. In general flow slides are not common, however, when a flow slide is initiated it takes place rapidly with little warning and is usually catastrophic. Therefore, in order to prevent such a disaster, an accurate assessment of post-earthquake slope stability accounting for soil shear strength reduction is demanded.

There is now considerable experimental evidence to show that very loose sand under cyclic or monotonic shearing exhibits significant reduction in strength associated with increase in pore water pressure. Also according to the literature, the behavior of dense sand during undrained shearing is predominately strain hardening, since the ultimate state strength is very large. However, this interpretation is based mainly on results of undrained triaxial compression tests (i.e. limited strain). Furthermore, after examining results of undrained triaxial compression tests on Toyoura sand presented by Ishihara (1993), Robertson and Fear (1997) concluded that for some sands very large strains are required to attain the ultimate state, and in some cases conventional triaxial equipment may not reach these large strains ($\varepsilon_a > 20\%$).

During recent years, results of undrained ring shear tests on soil specimens taken from sites where earthquake-induced landslides occurred as well as sandy soils, were reported in literature by Sassa and colleagues (Sassa, 1996; Sassa et al., 1997a; Wang, 1998; Wang et al., 2000; Sassa 2002). A central feature of these experiments is the phenomenon of sliding surface liquefaction, which may take place within the shear zone due to progressive increase in

excess pore water pressure with accumulated unidirectional shear displacement. Sliding surface liquefaction is a special kind of liquefaction; it differs from the normally understood (mass) liquefaction (Sassa 1996). According with the undrained ring shear tests results on sandy soils presented by Wang (1998), sliding surface liquefaction can be triggered in medium dense and dense specimens due to pronounced contractive behavior of the soil after reaching the failure condition.

Whereas small strains are required to trigger liquefaction in a very loose sand, the observed mechanism of sliding surface liquefaction is due to large unidirectional shear displacements and it is associated with soil failure, i.e., this phenomenon will not occur whether failure has not been initiated. In respect with earthquake-induced landslides, sliding surface liquefaction may not take place unless the driving shear stress will be able to drive the sliding mass after the earthquake has ceased. Hence, the immediate post-earthquake landslide mobility is directly affected by the amount of earthquake-induced loss of soil shear strength. An accurate assessment of shear strength reduction degree involves a correct estimation of earthquake induced permanent slope deformation.

The simplified procedure developed by Makdisi and Seed (1978), to estimate embankment deformation during earthquakes, has become a standard of practice in geotechnical engineering. However, for soils exhibiting sliding surface liquefaction a conventional seismic slope stability based on displacement approach, assuming a constant single value of yield acceleration, would result in unrealistic predictions. Therefore, the process of progressive soil softening / excess pore pressure generation with accumulated earthquake induced unidirectional slope displacement should be included in analysis. Consequently, a predictive model for the excess pore water pressure evolution is necessary in order to couple the mechanism of shear strength reduction with dynamic response analysis.

The intent of present research is to develop a numerical procedure capable of giving accurate predictions of the residual excess pore water pressure evolution in sandy soils subjected to cyclic loading, based on ring shear tests. The *residual excess pore water pressure* as defined in this paper, represents that component of excess pore water pressure which is independent of cyclic loading and builds up with accumulated unidirectional shear displacement due to soil tendency to undergo volume changes during monotonic shearing. Two types of experiments were conducted on sand, by a newly developed ring shear apparatus, aiming to determine: (1) the relationship between shear stress / displacement behaviors and the volume-change characteristics of sand under monotonic loading; and (2) the residual excess pore water pressure generation due to cyclic loading with initial shear stress. Since volume changes in drained shear can be considered as a mirror image of pore water pressure build-up during undrained shear, the results concerning the first type of experiments are essential in developing the following proposed methodology.

2. Ring Shear Apparatus and Tested Specimens

An intelligent ring shear apparatus (DPRI-Ver.6), developed and improved by Sassa and colleagues (Sassa, 1997), was employed in this study. A very detailed description of this testing device is given elsewhere (Wang and Sassa, 2000), and some particular aspects are also summarized in the following. The specimen represented in Fig. 1a is about 135 mm in height with an outer diameter of 350 mm and an inner diameter of 250 mm, respectively. The most important part of this ring shear apparatus is the undrained shear box shown in Fig. 1b, where the pore water pressure measurement system may also be noticed. Water-leakage proof is achieved by rolling two "O" rings on the upper loading plate, and pasting rubber edges on the two confining rings of the lower part of shear box. The pressure acting between upper rings and rubber edges is maintained constant during experiment through a gap control oil piston.

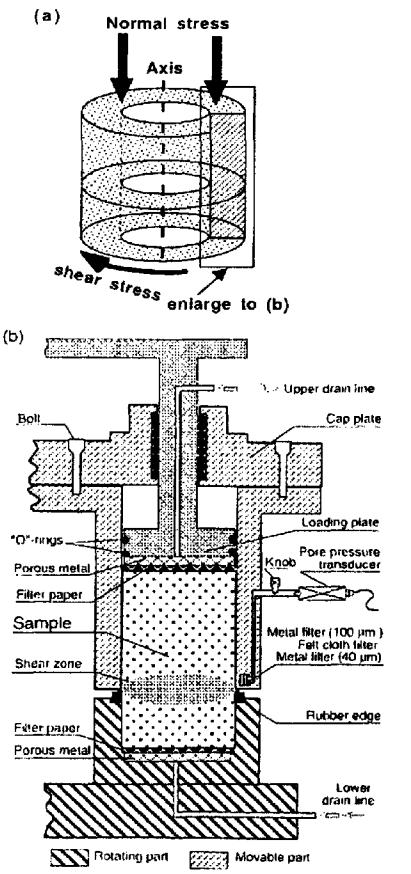

Fig. 1 Ring shear specimen (a) and half cross section of the undrained shear box (b) of the DPRI-6 ring shear apparatus (after Wang and Sassa, 2000a)

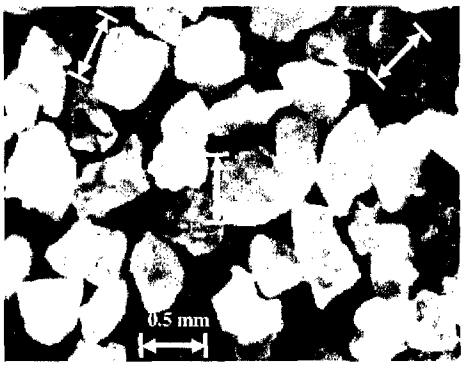

Fig. 2. Microscopic view of silica sand no. 6 (60x)

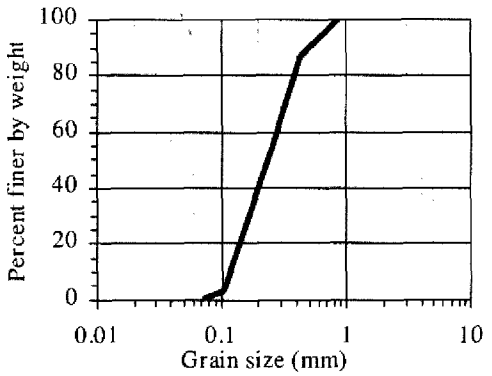

Fig. 3 Grain-size distribution of silica sand no. 6

The present study is concerned with ring shear tests on silica sand no. 6 (S6), which mainly consists of quartz (92%-98%) and a small amount of feldspar. Examination of S6 under an optical microscope revealed that the grains are subrounded to subangular, as shown in Fig. 2. Table 1 summarizes the results of a series of laboratory tests performed to determine the gradation, specific gravity and the maximum / minimum void ratio of S6. The grain size distribution of S6 is also illustrated in Fig. 3. It is seen from Fig. 3 that S6 is uniform, with grain sizes ranging from 0.07 to 0.8 mm and has no fines, therefore it may be classified as a poorly graded sand.

Table 1 Properties of silica sand no. 6

Mean grain size, D_{50} (mm)	0.25
Effective grain size, D_{10} (mm)	0.115
Uniformity coefficient, U_c	2.4
Maximum void ratio, e_{max}	1.16
Minimum void ratio, e_{min}	0.69
Specific gravity, G_s	2.66

3. Sample Preparation and Testing Procedure

The specimens were prepared by dry deposition method, that is, the oven dried sample fell into the shear box freely through a plastic bottle like a funnel, from the top of the upper ring. The saturation was accomplished by aid of carbon dioxide and de-aired water, after the sample had been poured in the shear box. The saturation degree was checked by calculating B_D value proposed by Sassa (1988) and given by Eq. (1):

$$B_D = \frac{\Delta u}{\Delta \sigma} \quad (1)$$

in which Δu stands for the increment of pore water pressure increase due to a change in total normal stress normally from 50 to 100 kPa, i.e., $\Delta\sigma$ = 50 kPa under undrained conditions. The specimen is assumed to be fully saturated when B_D > 0.95. All ring shear tests in this study have been carried out at a B_D > 0.95.

The experimental program included series of experiments on normally consolidated specimens at different effective normal stresses ranging from 147 kPa to 343 kPa.

3.1 Drained monotonic ring shear tests

The samples were normally consolidated and sheared after consolidation, in a drained monotonic manner, with a loading rate of shear stress of 1 kPa/sec, employing the medium rotating gear with a final shear speed of 32.3 cm/sec. Results of drained monotonic shearing are depicted in Fig. 4, for effective normal stress levels ranging from 147 to 294 kPa. The peak shear strength was mobilized at shear displacements between 12-20 mm. After mobilization of the initial peak, the soil exhibited displacement-softening behavior until the residual strength was attained at shear displacements between 400-500 mm. Subsequent shearing involved displacement-hardening toward a secondary peak attained at about 10 m shear displacement.

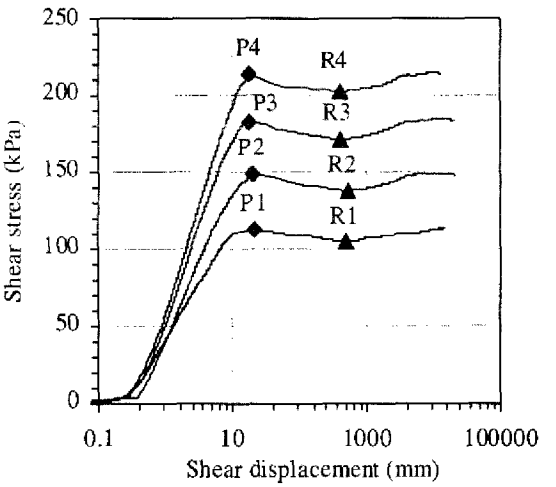

Fig. 4 Results of drained monotonic ring shear tests for normally consolidated silica sand no. 6 under effective stress levels of 147 kPa (e_c=0.97), 196 kPa (e_c=0.98), 245 kPa (e_c=0.96) and 294 kPa (e_c=0.94).

The evolution of sample height change in relation with shear displacement, illustrated in Fig. 5, indicates a contractive behavior during the entire shearing process. Peak and residual strength envelopes are also shown in Fig. 6. Both peak and residual strength envelopes are linear for the range of effective normal stresses considered, and show no apparent cohesion intercept.

The soil has a peak friction angle, $\phi'_p = 36^o$, and a residual friction angle, $\phi'_r = 34.5^o$. The small difference of only 1.5^o between peak and residual appears to be reasonable for a medium dense sand.

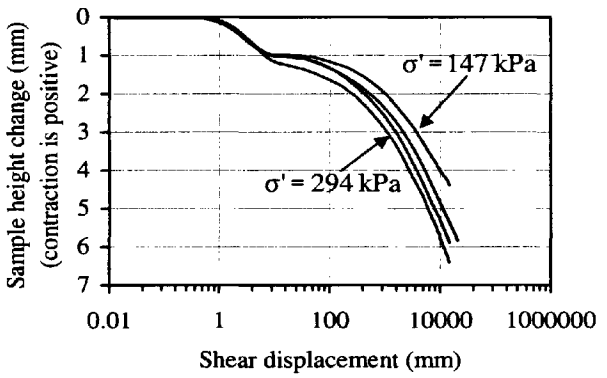

Fig. 5 Sample height change versus shear displacement relationship during drained monotonic shearing

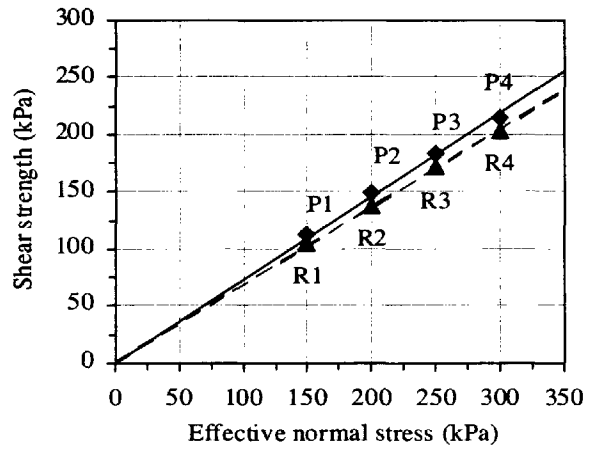

Fig. 6 Peak and residual failure envelopes for normally consolidated silica sand no. 6

3.2 Undrained cyclic loading ring shear tests

The undrained cyclic testing program was decided according to Fig. 7. In a first stage the initial stresses were enforced in order to simulate an infinite slope (Fig. 7a) with a gradient $\alpha = \tan^{-1}(0.5)$. After consolidation under an effective normal stress, $\sigma'^0 = \sigma^0$, the initial shear stress was increased under drained conditions to an initial value, $\tau^0 = \sigma^0 \cdot \tan(\alpha) = 0.5\sigma^0$. The stress points A, B, C and D, in Fig. 7b, are the initial stress conditions for the undrained cyclic loading tests performed in this study.

The initial stress level is defined by Eq. (2):

$$SL^0 = \frac{\tau^0}{\sigma'^0 \cdot \tan\phi'_p} \qquad (2)$$

It may be easily noticed that the initial stress level is the same for cases A, B, C, and D, with a value equal to 0.688.

After setting the initial stresses, the cyclic shear stress is applied, under undrained conditions, while maintaining constant the total normal stress, to reproduce a seismic force acting parallel to the sliding surface. A sine wave form of 0.1 Hz has been selected for cyclic shear stress, based on the facility and versatility of operation in the laboratory.

In order to reach the failure condition, the amplitude of seismic force coefficient was increased gradually at the beginning of each cycle, by a constant increment of 0.025, as illustrated in Fig. 7c. The total number of cycles employed in each experiment was set to 13.

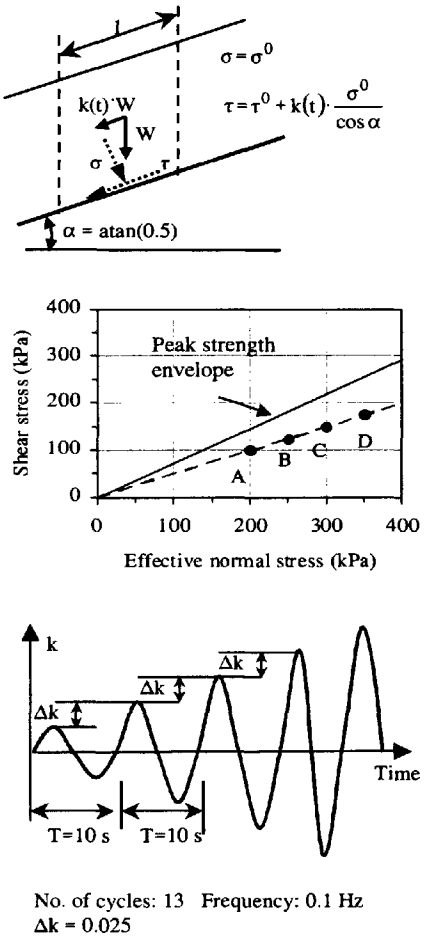

Fig. 7 Initial stress conditions (a), (b) and wave form of cyclic shear stress (c) for undrained cyclic loading ring shear tests

Typical results showing the shear stress and excess pore water pressure in relation with time and shear displacement, for the initial stress point B in Fig. 7b, are depicted in Figs. 8 and 9. It can be noticed that the available shear strength became smaller than initial static shear stress within the 9th cycle of dynamic loading. From that point the shear displacement developed unidirectionally associated with accelerated motion. After failure the excess pore water pressure built up gradually, resulting in progressive reduction of soil shear strength and, finally, sliding surface liquefaction, when steady state was attained.

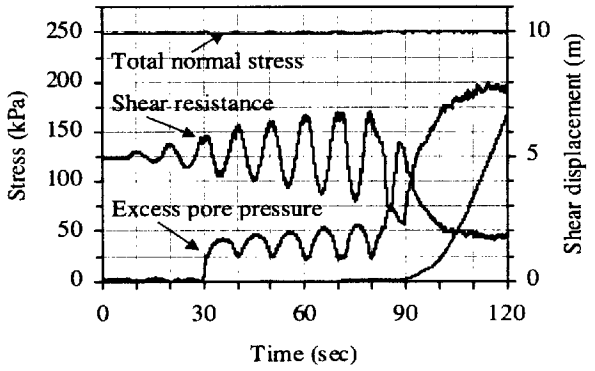

Fig. 8 Time series data of a typical undrained cyclic loading ring shear test under a constant total normal stress level of 245 kPa (e_c=0.96)

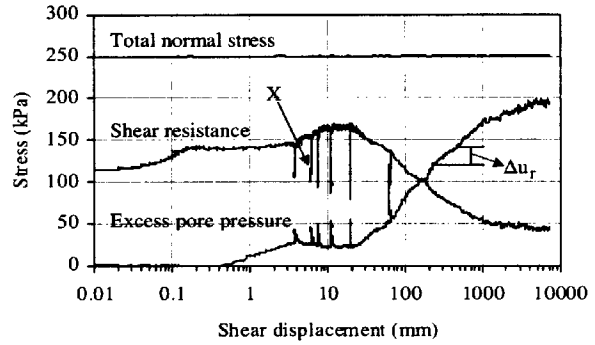

Fig. 9 Shear resistance and excess pore pressure versus shear displacement for time series data presented in Fig. 8

4. Components of Excess Pore Water Pressure Increment

The excess pore water pressure increment, Δu, between two consecutive load steps, in an undrained cyclic loading ring shear test, consists of a cyclic component, Δu_c, induced by dynamic stresses, and a residual component, Δu_r, due to potential of volume reduction with progress of shear displacement. The cyclic component, Δu_c, may be written as follows:

$$\Delta u_c = \Delta u_c(\Delta\sigma) + \Delta u_c(\Delta\tau_{UR}) \quad (3)$$

The first term in Eq. (3) represents the excess pore water pressure increment due to cyclic normal stress increment, $\Delta\sigma$, and it can be assessed by Eq. (4):

$$\Delta u_c(\Delta\sigma) = B_D \cdot \Delta\sigma \quad (4)$$

with B_D defined by Eq. (1). In respect with this pore pressure component, all cyclic loading ring shear tests introduced in the preceding section were performed under constant total normal stress, therefore, $\Delta u_c(\Delta\sigma) = 0$.

The latter term of Eq. (3) stands for the excess pore water pressure increment due to shear displacement reversal and it is clearly depicted in Fig. (10) representing an expanded detail of the unloading-reloading path, X, in Fig. (9). Since reversals of shear displacement may occur only throughout the yielding stage of shearing, the second term of Eq. (3) will be omitted for the post-failure behavior.

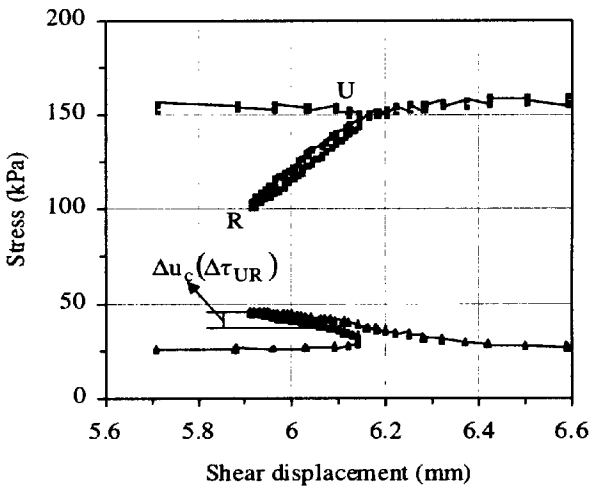

Fig. 10 Enlarged detail of the unloading-reloading loop, X, in Fig. 9

The residual excess pore water pressure increment, Δu_r, schematically illustrated in Fig. 9, is independent of cyclic loading and builds up with accumulated unidirectional shear displacement. Typically, for soils exhibiting sliding surface liquefaction, additional loading beyond the peak strength is associated with gradual increase of residual excess pore water pressure resulting in progressive loss of shear strength due to accelerated motion.

The cyclic loading conditions in slopes during earthquakes, usually are not substantial enough to reverse the shear stress direction, which is the soil exhibits in most cases unidirectional strain. Hence, the residual excess pore water pressure is a key factor for the mobility of a landslide, during and after a seismic excitation. Therefore, an accurate assessment

of this parameter is of great importance for landslide researchers. In this context, a numerical procedure to estimate the residual excess pore water pressure developed in sand under cyclic loading is proposed.

5. Computational Model

When shear stresses are applied to saturated sandy soils, and if the loading conditions or soil properties do not allow for drainage, the water in the system is not expelled from the soil voids during loading. Consequently, the soil tendency to undergo shear induced volume changes reflects in variations of pore water pressure during undrained loading. The basic concept of the following formulation is to estimate the equivalent stress increment transferred from the soil skeleton onto the water, between two consecutive time moments during undrained shearing.

The necessary input parameters for the computational procedure are summarized in Table 2 according with, additional explanations will be given below for R_c parameter and $(\Delta H_n$ v.s. $L)$ relationship.

Table 2 Model input data

Parameter	Symbol
Initial effective normal stress	σ'^0
Initial shear displacement	L^0
Pore pressure parameter	B_D
One dimensional rebound coefficient	R_c
Normalized change in sample height v.s. shear displacement relationship	ΔH_n vs L

Figure 11 illustrates results of a consolidation test performed under different effective normal stress levels in the ring shear box for dry silica sand no.6. Considering two points, A and B, located on the unloading path after consolidation under a certain effective normal stress level (Fig. 11), the one dimensional rebound coefficient, R_c, may be expressed by Eq. (5):

$$R_c = \frac{\Delta H_B - \Delta H_A}{\ln(\sigma'_B) - \ln(\sigma'_A)} \tag{5}$$

with ΔH_A and ΔH_B representing the sample height changes at the effective normal stress levels σ'_A and σ'_B during unloading. For computational purposes an average value of R_c was considered based on the one dimensional compression test results presented in Fig. 11.

The normalized change in sample height is defined by Eq. (6):

$$\Delta H_n = \frac{\Delta H}{\left(\frac{\sigma'}{p_a}\right)^n} \tag{6}$$

in which ΔH is the sample height change during drained monotonic shearing under a constant effective normal stress, σ' (Fig. 5). The symbol p_a in Eq. (6) stands for the atmospheric pressure assumed to be 101.3 kPa. The main advantage of $(\Delta H_n$ v.s. $L)$ diagram is that, for a certain value of parameter n, an unique relationship may be drawn for any level of effective normal stress. Hence, in order to avoid significant errors inherent with an interpolation process, $(\Delta H_n$ v.s. $L)$ representation is more appropriate for numerical analysis. As illustrated in Fig. 12, the experimental $(\Delta H$ v.s. $L)$ curves from Fig. 5, gather into a single relationship for n = 0.5.

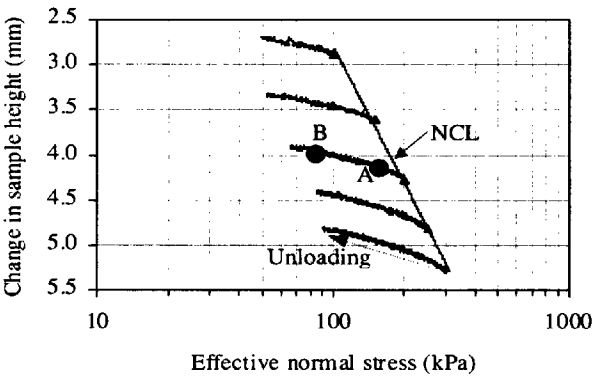

Fig. 11 Results of uniaxial compression test performed in the ring shear box on silica sand no. 6

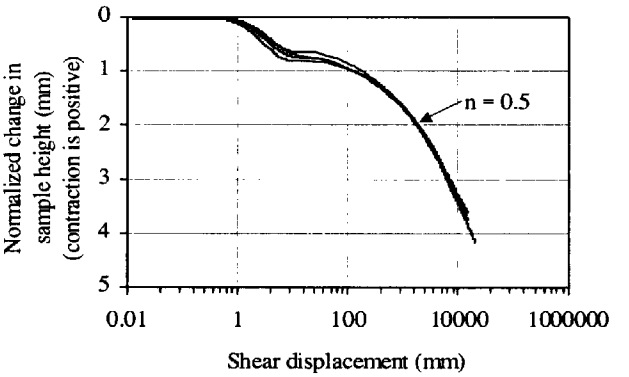

Fig. 12 Normalized change in sample height versus shear displacement relationship for n = 0.5

5.1 Procedure for incremental analysis

The flow of computational steps, for two consecutive shear displacement readings L^i and L^{i+1}, is shown in Fig. 13 and described as follows:

Step 1: Extract the normalized change in sample height, ΔH_n^{i+1}, corresponding to L^{i+1}, based on the diagram in Fig. 12.

Step 2: Calculate the increment of sample height change, $\left(\Delta H^{i+1} - \Delta H^i\right)$, based on Eq. (6), assuming a constant value of effective normal stress equal to σ'^i.

Step 3: Calculate the increment of equivalent decrease in effective normal stress, $\Delta\sigma'_{equiv}$, according with Eq. (5).

Step 4: Calculate the residual excess pore water pressure, u_r^{i+1}, and the effective normal stress, σ'^{i+1}, based on the value of $\Delta\sigma'_{echiv}$ estimated at Step 3.

Step 5: Repeat steps 1 to 4 for the next two consecutive shear displacement readings, L^{i+1} and L^{i+2}.

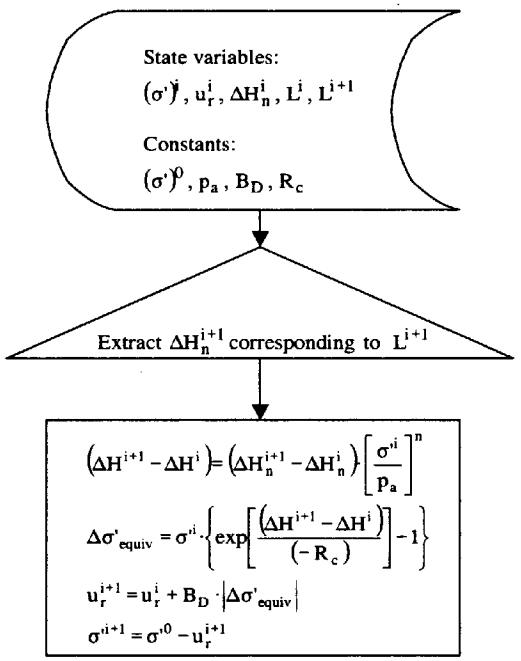

Fig. 13 Flowchart of computational procedure

5.2 Model calibration

The proposed model was utilized to estimate the residual excess pore water pressure generated in the undrained cyclic loading ring shear tests A, B, C, D introduced in section 3.2. An interpretation of the residual excess pore water pressure pattern, obtained by a straightforward implementation of the previous numerical procedure showed that, the calculated pore pressure developed more quickly with accumulated shear displacement than experimental values.

A possible explanation relies on the experimental nature of parameter R_c used in the analysis and defined by Eq. (5). As mentioned in section 5.1, a constant value of R_c was assumed in computations, based on the results of uniaxial compression tests carried out on dry sand in the ring shear box. Hence, R_c quantifies the soil deformability within the entire volume of tested specimen, due to variations in effective normal stress. Nevertheless the mechanism of sample height change during drained monotonic shearing is far more complex than soil behavior during a simple compression test, being associated with phenomena that take place especially within the shear zone, which is a core of limited extension inside the specimen. Therefore, errors in the calculated residual excess pore water pressure are likely to occur when R_c values from uniaxial compression tests are used in computations.

Accordingly, a correction factor, C_{ur}, is introduced in this study, and defined as:

$$C_{ur} = \frac{u_r^m}{u_r} \tag{7}$$

where u_r^m and u_r are the experimental and calculated residual excess pore water pressure.

Figure 14 shows the scattering in correction factors for the undrained cyclic loading ring shear tests A, B, C, D presented in section 3.2. In this representation the correction factors follow almost the same pattern in relation with shear displacement, independent of the initial effective normal stress level. For computational purposes, this trend may be approximated by a bi-logarithmic relationship, identified with $\overline{C}_{ur}$ in Fig. 14. The corrected residual excess pore water pressure, $\bar{u}_r$, is obtained by:

$$\bar{u}_r = \overline{C}_{ur} \cdot u_r \tag{8}$$

where u_r stands for the residual excess pore water pressure estimated by the numerical procedure described in section 5.1.

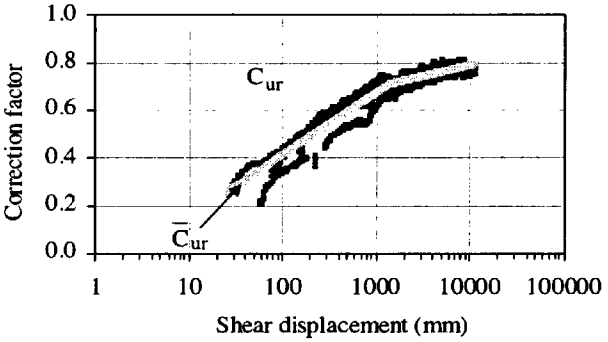

Fig. 14 Correction factor in relation with shear displacement

5.3 Comparison with experimental results

The proposed methodology was employed to predict the evolution of the residual excess pore water pressure during an undrained cyclic loading ring shear test on silica sand no. 6. In this experiment both total normal stress and cyclic shear stress were applied in a cyclic manner. The sample preparation

and saturation were done according to the procedure summarized in chapter 3. After consolidation under an effective normal stress of 245 kPa, the shear stress was slowly increased, under drained conditions, to an initial value $\tau^0 = 0.5 \cdot \sigma^0$, aiming to reproduce the initial stress conditions illustrated by point B in Fig. 7b. This stress state is consistent with the initial conditions for an hypothetical infinite slope with a steepness of 1:2 sketched in Fig. 15. Hence, an initial stress level, $SL^0 = 0.688$, was achieved, the same as that for the undrained cyclic loading ring shear tests summarized in Fig. 7.

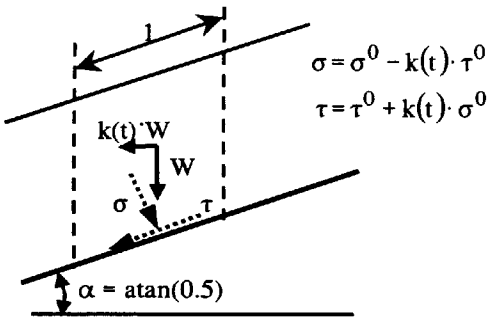

Fig. 15 Static and seismic stress conditions for the undrained cyclic loading ring shear test illustrated in Fig. 16

Unlike the experiments in section 3.2, in this case a seismic force acting horizontally was assumed (Fig. 15). However, the wave form of the seismic coefficient, k, is identical with that represented in Fig. 7c. Time series data of the undrained cyclic loading ring shear test are depicted in Fig. 16.

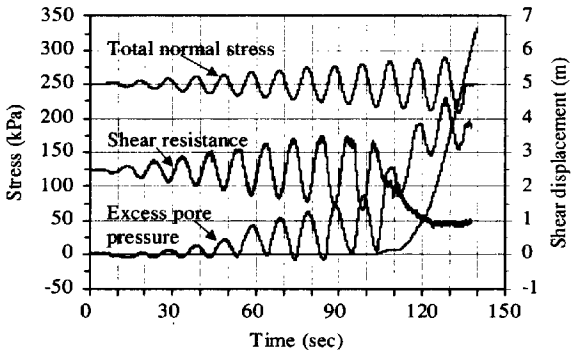

Fig. 16 Time series data of the undrained cyclic loading ring shear test (e_c=0.96)

Figure 17 shows the predicted residual excess pore water pressure, $\bar{u}_r$. On the same diagram was represented also the estimated excess pore water pressure computed as the sum between predicted residual excess pore water pressure, u_r, and cyclic excess pore water pressure, $u_c(\sigma)$, expressed by Eq. (4). The results indicate a good agreement between predicted and experimental values of the excess pore water pressure after failure. However, underestimations in calculated excess pore water pressure are to be noticed throughout the yielding stage prior to failure, since the cyclic excess pore water pressure accompanying shear displacement reversals, $u_c(\tau_{UR})$, was not considered in computations.

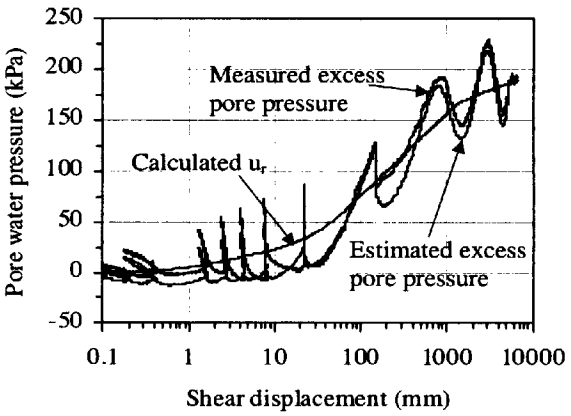

Fig. 17 Estimated and measured excess pore pressures

6. Conclusions

Undrained cyclic loading and drained monotonic ring shear tests on sand were examined and, based on the experimental observations, a simple procedure to evaluate the residual excess pore water pressure evolution during cyclic loading under undrained conditions was formulated and calibrated against the experimental results. Consequently, a correction factor was introduced based on comparisons between predicted and experimental values of the residual excess pore water pressure. Since this study is related to results of undrained cyclic loading ring shear tests with the same initial stress level (SL^0=0.688), the correction factor affecting the predicted residual excess pore water pressure may be subjected to changes according to SL^0.

The procedure has been validated through comparison with undrained cyclic loading ring shear test results simulating an infinite slope, driven by a seismic force acting horizontally, thus both total normal stress and shear stress were applied in a cyclic manner.

The proposed approach is just under a preliminary stage and comprehensive research based on undrained cyclic loading ring shear tests with various initial stress levels are necessary in order to extend the applicability of the method.

Acknowledgments

The authors wish to thank to Dr. Gonghui Wang, Research Fellow of Landslide Section of Disaster Prevention Research Institute, Kyoto University, for

his valuable suggestions and guidance in conducting undrained cyclic loading ring shear tests. Also the support provided by Mr. Kumahiro Kondo in fixing the trouble shootings of ring shear apparatus is greatly appreciated.

References

Ishihara, K. (1993): Liquefaction and flow failure during earthquakes, The 33rd Rankine Lecture. *Geotechnique*, Vol. 43, No. 3, pp. 351-415

Kramer, S.L. (1996). *Geotechnical Earthquake Engineering*, Prentice Hall, Inc., Upper Saddle River, New Jersey, 653 pp

Makdisi, F.I. and Seed, H.B. (1978): Simplified procedure for estimating dam and embankment earthquake-induced deformation. *J. Geotech. Eng. Div., Am. Soc. Civ. Eng.*, 104(GT7), pp. 849-867.

Robertson, P.K. and Fear, C.E. (1997): Liquefaction of sands and its evaluation. Keynote Lecture. *Proc. IS-TOKYO '95 / The 1st Intl. Conf. On E.q. Geotech. Engrg.*, (ed. by Balkema, A.A.), November 14-16, 1995, Tokyo, Vol. 3, pp. 1253-1289.

Sassa, K. (1988): Motion of Landslides and Debris-Flows- Prediction of hazard area. *Report for Grant-in-Aid for Scientific Research by Japanese Ministry on Education, Science and Culture*, Project No. 61480062, pp. 15.

Sassa, K. (1996): Prediction of earthquake induced landslides. Special Lecture of 7th International Symposium on Landslides, *"Landslides"*, Rotterdam: Balkema, 1, 115-132.

Sassa, K. (1997): A new intelligent type of dynamic loading ring-shear apparatus. *Landslide News*, No. 10, pp. 33.

Sassa, K., Fukuoka, H. and Wang F.W. (1997a): A geotechnical simulation test on the Gamahara torrent debris flow with ring shear apparatus (in Japanese). *Journal of the Earth*, Vol. 19, No. 10, pp. 645-651.

Sassa, K. (2002): Mechanism of rapid and long traveling flow phenomena in granular soils. *Proc. Int. Symp. on Landslide Risk Mitigation and Protection of Cultural and Natural Heritage*, Vol. 1, pp. 11-29.

Wang, F.W. (1998): An experimental study on grain crushing and excess pore pressure generation during-shearing of sandy soils- A key factor for rapid landslide motion. Ph.D. Thesis. Kyoto University.

Wang, F.W., Sassa, K. and Fukuoka, H. (2000): Geotechnical simulation test for the Nikawa landslide induced by January 17, 1995 Hyogoken-Nambu earthquake. *Soils and Foundations*, Vol. 40, No. 1, pp. 35-46.

Wang, F.W. and Sassa, K. (2000a): Relationship between grain crushing and excess pore pressure generation by sandy soils in ring-shear tests. *Journal of Natural Disaster Science*, Vol. 22, No. 2, pp. 87-96.

Wang, G. and Sassa, K. (2000): Fluidization behavior of sands based on ring shear tests: effects of grain size and fine-particle content. *Disaster Prevention Research Institute Annuals, Kyoto University*, No. 43 B-1, pp. 141-160.

要旨

本研究は，砂質土の繰り返し載荷時に発生する残留過剰間隙水圧を数値的に予測する手法に関するものである．リングせん断試験機による砂の非排水繰り返し載荷試験と排水・定速度せん断試験結果を検討したところ，非排水せん断時の残留過剰間隙水圧は排水・定速度せん断時の供試体高さの変化に関係することがわかった．したがって，せん断とともに発生する残留過剰間隙水圧の計算式を提案し，実験結果と比較して検証した．その結果，垂直応力とせん断応力ともに繰り返し載荷した条件下の試験では上記計算式は妥当であることが証明された．提案した予測法は基本的な砂の物性値を用いて残留過剰間隙水圧の理論的な数値予測を行うものであり，動的応答解析における間隙水圧上昇予測も可能となる．

キーワード：過剰間隙水圧，残留過剰間隙水圧，リングせん断試験，砂質土，定速度せん断試験